5 Occurrence of excess ^{40}Ar in retrograde metamorphic amphiboles investigated by joint $^{40}Ar/^{39}Ar$ *in vacuo* crushing and stepwise heating*

5.1 Introduction

Although it is generally accepted that continental subduction is characterized by a scarcity of fluid when compared with subduction of oceanic crust, a considerable amount of aqueous fluid can still be released. A significant and abrupt decrease in either temperature or pressure along the retrograde part of the *P-T* loop may trigger recrystallization of hydrous and hydroxylated minerals, and the decrepitation of primary fluid inclusions to release fluid (Zheng, 2004; Hermann et al., 2006). As a result, amphibolite and greenschist facies retrogression of eclogites and granulites, and even syn-exhumation magmatism are likely to be caused by aqueous fluid flow during exhumation of deeply-subducted continental crust (Baker et al., 1997; Franz et al., 2001; Fu et al., 2003).

Several groups have studied the fluid inclusions and petrological phase relations of HP/UHP metamorphic rocks to constrain the origin, the volume and the elemental and hydrogen and oxygen isotopic composition of these metamorphic fluids (Li et al., 2001b; Touret, 2001; Xiao et al., 2002; Fu et al., 2003; Zheng et al., 2003). These studies have greatly improved our understanding of the nature and effect of fluid activity during exhumation of deeply-subducted continental crust. Based on studies involving stable isotopes, fluid inclusions and petrological phase relationships of Sulu-Dabie orogenic UHP metamorphic rocks, (Zheng, 2004) proposed that the fluid activity during the exhumation of deeply subducted continental crustal is characterized by pervasive fluid flow resulting in amphibolite-facies retrogression, and channelized fluid flow leading to the formation of HP quartz veins within eclogites. In many other UHP metamorphic belts, fluid inclusion studies suggest that minerals in eclogites and their retrograde products normally contain a variety of types of fluid inclusions, and there is some correlation between metamorphic grade and metamorphic fluid composition (Andersen et al., 1989; Andersen et al., 1993; Philippot et al., 1995; Han and Zhang, 1996; Touret, 2001; Zhang et al., 2011b). In other words, fluid flow in UHP metamorphic terranes is generally considered to be episodic.

In comparison with research on the chemistry and isotopic composition of metamorphic fluids, it is more difficult to constrain the timing of fluid infiltration during retrogression of UHP metamorphic rocks. Rather than attempting to indirectly date the quartz sample by using, e.g., the Rb-Sr isotopic decay system (Wang et al., 2000a; Wang et al., 2003) or to directly date metamorphic minerals such as garnet and amphibole by extracting gas from fluid inclusions for $^{40}Ar/^{39}Ar$ dating (Qiu and Wijbrans, 2006; 2008; Qiu et al., 2010), perhaps

* This chapter was part of the Chinese version of the thesis.

the greatest insights into the age of fluid activity in UHP rocks have been attained from studies of accessory minerals like zircon and rutile associated with quartz veins in eclogite-facies rocks (Gao et al., 2006; Zheng et al., 2007; Wu et al., 2009b; Zong et al., 2010; Wang et al., 2011; Chen et al., 2012). The ^{40}Ar/^{39}Ar *in vacuo* crushing method has been utilized in several studies of fluid inclusion-rich light-colored rocks and minerals such as chert (Alexander, 1975; Wang et al., 1988), vein quartz (Kelley et al., 1986; Turner, 1988; Qiu, 1996; Kendrick et al., 2001; Kendrick et al., 2006) and feldspar (Burgess et al., 1992; Turner and Bannon, 1992; Harrison et al., 1993; Burgess and Parsons, 1994), with the aim of investigating either the paleo-atmospheric ^{40}Ar/^{36}Ar ratio or the source and halogen chemistry of fluid inclusions. In addition to that, sulphide minerals like pyrite and sphalerite (Phillips and Miller, 2006; Qiu and Jiang, 2007; Jiang et al., 2012), volatile-rich metamorphic minerals like scapolite from hydrothermal deposits (Kendrick and Phillips, 2009), and low-potassium minerals like garnet from HP/UHP metamorphic rocks (Qiu and Wijbrans, 2006; 2008) have been analysed with some success using this dating method. In a critique of this method, Kendrick and Phillips (2009) argued that a significant amount of lattice-hosted noble gas from scapolite can be released during prolonged crushing, but a number of studies has indicated that crushing has very little effect on the gas component that is trapped within the crystal lattice (Dunlap and Kronenberg, 2001; Qiu and Wijbrans, 2008; Qiu et al., 2010; Jiang et al., 2012; Bai et al., 2013). Therefore, a combination of ^{40}Ar/^{39}Ar dating during progressive crushing and stepwise heating of the crushed powder could provide an opportunity to distinguish the gas components trapped inside fluid inclusions and on the grain boundaries of solid inclusions from those within the crystal lattice (Villa, 2001; Kelley, 2002).

Here, we report a ^{40}Ar/^{39}Ar study of amphibole from garnet amphibolites from the Yuka terrane, north Qaidam, western China. By applying the *in vacuo* crushing and stepwise heating ^{40}Ar/^{39}Ar techniques, we have been able to extract trapped argon from fluid inclusions and grain boundaries of solid inclusions, as well as from the crystal lattice of the metamorphic amphiboles. We use Ar isotopic studies to: (1) constrain the timing of fluid flow and amphibolite-facies retrogression of Yuka eclogite; (2) reveal the thermal history of these UHP rocks; and (3) identify extraneous ^{40}Ar when they are present.

5.2 Sample description

The samples used in this study for ^{40}Ar/^{39}Ar dating are amphiboles from two garnet amphibolites (09NQ13 and 09NQ29). Tow garnet amphiboles were collected from outcrops on the northern bank of the Yuka River, Yuka terrane.

Sample 09NQ13 was taken from a 1×0.6 m lens-shaped garnet amphibolite block hosted by muscovite schist. It is characterized by medium to coarse-grained massive structure, and consists of amphibole (~60%), clinozoisite (~10%), epidote (~10%), plagioclase (~5%), quartz (~5%), garnet (~5%), symplectites (Amp+Pl, ~5%) with minor biotite and titanite (Figure 5.1a).

Amphibole crystals are lepidoblastic with variable grain size from 1 to 5 mm with biotite, plagioclase and quartz as inclusions. Amphiboles are classified as edenite and magnesio-hornblende (c.f., Leake et al., 1997) with K/Ca ratios ranging from 0.08 to 0.11 with an average of 0.1.

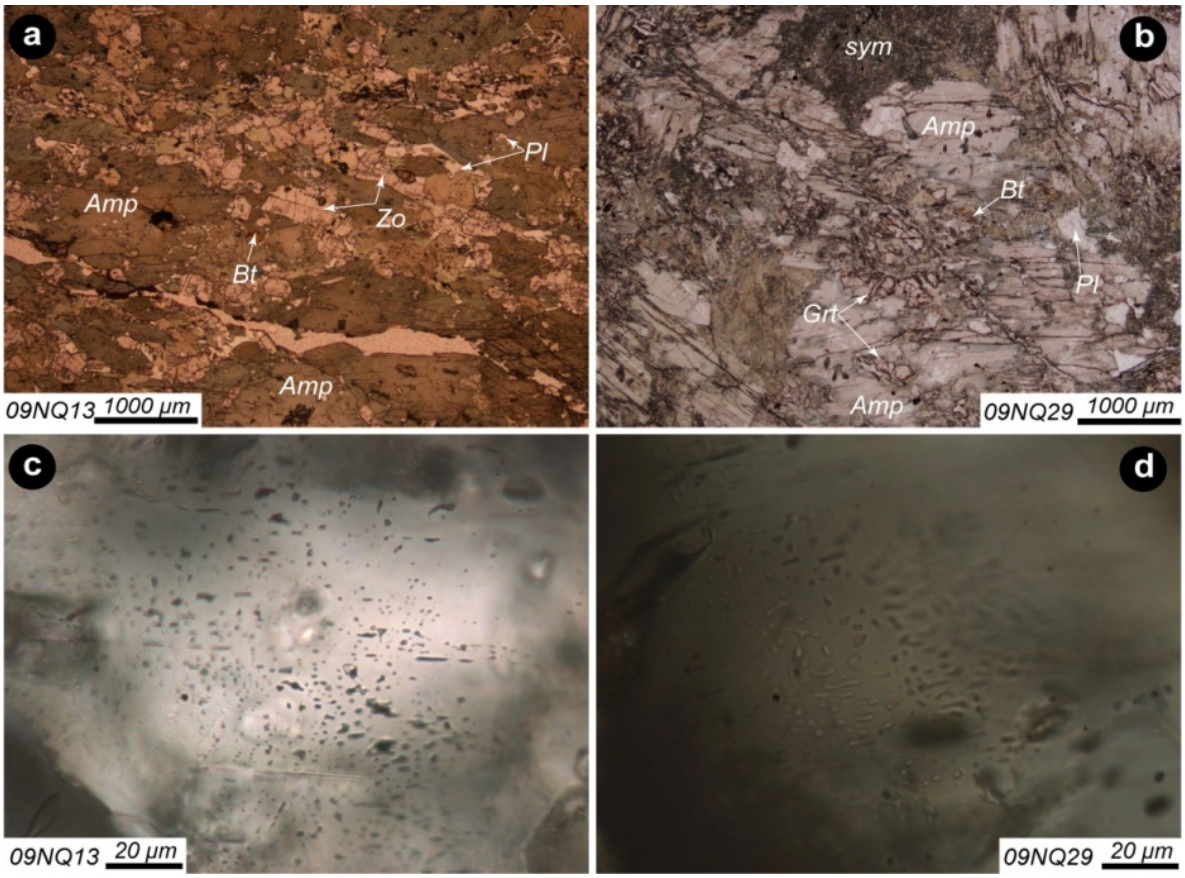

Figure 5.1 Photomicrographs in plane-polarized light (PPL) showing the textural relationships of amphibolites from the Yuka terrane. (a): euhedral to subhedral amphiboles contain zoisite, biotite and plagioclase as inclusions; (b): garnet relics occur as inclusions in coarse-grained amphibole. (c and d): primary fluid inclusions are randomly distributed with irregular, elongated and tubular shapes in amphibole.

Sample 09NQ29 is obtained from a garnet amphibolite lens and displays a gradual transition from eclogite-facies to amphibolite-facies mineralogy, with fresh eclogite preserved in the core. It is composed of amphibole (~60%), symplectites (Amp+Pl, ~10%), garnet (~10%) epidote (~10%) and plagioclase (~10%), with minor chlorite, titanite and biotite (Figure 5.1b). Garnet crystals display subhedral granular texture with grain sizes from 0.5 to 1 mm. Amphibole, which is characterized by intense alteration along the rim, shows lepidoblastic texture with grain sizes from 1 to 3 mm and normally contains mineral inclusions such as garnet, chlorite, biotite and plagioclase. Amphiboles are classified as winchite, barroisite, magnesio-hornblende and tschermakite (Leake et al., 1997) with K/Ca ratios ranged from 0.01 to 0.04 with an average of 0.03.

Preliminary petrographic observations have been carried out on polished amphibolite thin sections. Most of the fluid inclusions in the amphiboles are primary and small in size (*ca.* 0.5-3 μm), and are randomly distribute and characterized by irregular, tubular and elongated shapes (Figure 5.1c and d). Secondary fluid inclusions in amphibole were identified in healed fractures cross-cutting grain boundaries and growth zones, and generally bigger than primary types in size.

5.3 Results

Crushing *in vacuo* and stepwise heating of the powder residues experiments were carried out in an in-house designed crushing apparatus that was connected to a three stage extraction line and a quadrupole mass spectrometer (Schneider et al., 2009) in the argon isotope laboratory in VU University Amsterdam. Samples were loaded into a 40 cm long, 4 cm diameter Inconel® tube and crushed by an iron pestle that is lifted and dropped with a frequency of one time per second (1 Hz) using external electromagnet-control. The extracted gases were exposed to a cold trap filled with liquid nitrogen (kept at *ca.* – 90 °C), and then purified at 250 °C by a Fe/V/Zr getter pump and 450 °C by a Zr/Al getter pump. To analyze residues in stepwise heating experiments, the crusher tube was rotated 90 degrees and horizontally put into an externally temperature-controlled oven.

The ^{40}Ar/^{39}Ar analytical results are listed in Table 5.1 and Table 5.2. Age spectra and isochrons for each of the samples are plotted in Figure 5.2. All errors are reported at the 2σ confidence level in the text and figures.

Table 5.1 Complete ^{40}Ar/^{39}Ar *in vacuo* crushing data

Step	Pestle drop numbers.	$^{36}Ar_{air}$	$^{37}Ar_{Ca}$	$^{38}Ar_{Cl}$	$^{39}Ar_{K}$	$^{40}Ar^{*}$	Age ± 2σ (Ma)	$^{40}Ar_{K}$ (%)	^{39}Ar (%)	K/Ca(±2σ)
(a).Amphibole 09NQ13Amp, by crushing in vacuo, J = 0.005037										
1	6	81.1	446.6	4.6	68.7	304119.5	5679.4 ± 85.8	92.70	0.09	0.066 ± 0.047
2	12	108.1	929.4	9.4	176.9	673953.7	5421.2 ± 19.0	95.47	0.22	0.082 ± 0.028
3	20	97.8	1271.6	12.9	283.7	775021.5	4856.4 ± 18.6	96.41	0.36	0.096 ± 0.030
4	30	93.0	1601.5	13.4	468.0	838379.4	4158.2±16.8	96.83	0.59	0.126 ± 0.031
5	50	103.2	2657.3	12.4	730.9	932439.3	3617.1 ± 9.0	96.83	0.93	0.118 ± 0.020
6	70	68.7	3424.0	9.2	808.1	650709.2	2923.6 ± 9.9	96.97	1.02	0.101 ± 0.013
7	90	115.9	3357.0	7.9	939.9	601531.2	2599.2 ± 5.9	94.61	1.19	0.120±0.024
8	120	171.9	4293.8	4.5	1328.8	552008.6	2036.8 ± 8.2	91.58	1.68	0.133 ± 0.022
9	150	116.1	6380.9	8.9	1810.6	585617.9	1744.0 ± 6.0	94.47	2.30	0.122 ± 0.015
10	180	107.6	7924.5	9.1	2369.9	573155.5	1437.3 ± 5.0	94.74	3.00	0.129 ± 0.015
11	200	55.4	2502.4	2.6	975.4	146556.1	1016.6 ± 8.5	89.95	1.24	0.168 ± 0.029
12	220	54.5	6943.7	5.9	2248.2	303253.4	935.3 ± 5.3	94.95	2.85	0.139 ± 0.015
13	220	51.7	8455.2	8.7	2698.9	323518.6	852.2 ± 3.1	95.49	3.42	0.137 ± 0.016
14	240	50.2	9484.2	4.8	3293.4	317490.0	714.1 ± 3.2	95.54	4.18	0.149±0.019
15	300	57.8	9784.4	9.0	3442.1	280844.5	621.1 ± 2.7	94.27	4.36	0.151 ± 0.016
16	320	64.1	6893.2	4.4	2494.9	182264.9	565.3 ± 3.4	90.58	3.16	0.156 ± 0.020
17	340	2.3	4064.6	0.0	1572.9	107101.1	532.0 ± 4.8	99.37	1.99	0.166 ± 0.021
18	380	45.5	10569.4	0.0	3810.8	268824.7	548.5 ± 1.9	95.23	4.83	0.155 ± 0.017
19	400	5.5	9269.7	5.9	3194.8	213169.3	522.7 ± 2.8	99.25	4.05	0.148 ± 0.018
20	410	55.8	11453.9	5.2	4105.8	269922.7	516.0 ± 1.7	94.25	5.21	0.154 ± 0.017
21	410	37.5	12552.3	4.6	4493.6	298482.5	520.7 ± 1.6	96.42	5.70	0.154 ± 0.017

Table 5.1 continue

22	420	76.4	12285.6	7.2	4268.4	270168.1	499.3 ± 1.2	92.28	5.41	0.149 ± 0.019
23	440	81.9	12934.5	2.0	4432.6	278713.2	496.4 ± 1.1	92.01	5.62	0.147 ± 0.017
24	450	65.6	12842.5	15.4	4435.4	277570.4	494.3 ± 1.3	93.47	5.62	0.149 ± 0.018
25	460	64.2	13449.8	13.1	4084.9	252624.7	489.2 ± 1.9	93.01	5.18	0.131 ± 0.014
26	480	39.9	7142.9	5.2	2404.6	150354.0	494.0 ± 1.8	92.72	3.05	0.145 ± 0.017
27	460	26.2	11653.1	8.1	3747.9	228616.0	483.4 ± 1.4	96.73	4.75	0.138 ± 0.017
28	440	27.2	9699.8	3.5	3008.3	183705.2	483.8 ± 2.8	95.81	3.81	0.133 ± 0.016
29	420	8.3	9870.2	6.1	2906.4	171993.5	470.7 ± 1.7	98.59	3.68	0.127 ± 0.016
30	460	34.6	9083.8	6.5	2581.3	157868.6	484.5 ± 1.6	93.92	3.27	0.122 ± 0.015
31	480	3.6	9690.5	2.5	2816.2	167264.5	472.2 ± 1.6	99.36	3.57	0.125 ± 0.018
32	500	4.9	9602.7	10.2	2879.4	170910.1	471.9 ± 2.0	99.17	3.65	0.129 ± 0.016
(b).Amphibole 09NQ29Amp, by crushing in vacuo, J = 0.005031										
1	6	70.3	258.7	5.4	47.9	148625.8	5059.6 ± 111	87.74	0.11	0.080 ± 0.061
2	12	99.8	688.8	6.3	101.7	385123.2	5400.4 ± 88.2	92.89	0.23	0.063 ± 0.028
3	20	161.0	1133.4	3.3	173.1	570836.1	5163.7 ± 40.3	92.31	0.38	0.066 ± 0.018
4	30	110.6	1392.0	10.1	228.1	492674.3	4454 ± 19.8	93.78	0.51	0.070 ± 0.016
5	30	48.1	954.2	6.9	149.0	308919.8	4386.3 ± 50.1	95.60	0.33	0.067 ± 0.013
6	40	53.6	1316.8	6.4	203.4	292197.9	3793.6 ± 23.4	94.86	0.45	0.066 ± 0.015
7	50	45.1	1832.1	5.5	223.6	263556.9	3484.3 ± 26.8	95.19	0.50	0.052 ± 0.007
8	70	82.3	2112.6	6.6	306.6	294780.4	3174.6 ± 28.4	92.38	0.68	0.062 ± 0.010
9	90	88.9	2568.3	5.7	364.8	327041.1	3070.6 ± 20.7	92.57	0.81	0.061 ± 0.008
10	100	104.3	2212.3	4.7	432.0	274685.4	2581.0 ± 9.2	89.91	0.96	0.084 ± 0.014
11	120	125.2	3964.3	9.4	601.3	320009.8	2342.2 ± 8.2	89.64	1.33	0.065 ± 0.009
12	150	108.2	2974.1	0.1	528.8	213291.0	1992.7 ± 11.2	86.96	1.17	0.076 ± 0.011
13	170	118.8	5386.3	0.0	823.5	229148.0	1573.6 ± 10.6	86.72	1.83	0.066 ± 0.007
14	190	99.0	6075.2	2.0	1088.2	274258.0	1471.8 ± 6.5	90.36	2.41	0.077 ± 0.009
15	210	98.2	7527.4	3.2	1333.1	256061.0	1215.0 ± 6.4	89.82	2.96	0.076 ± 0.008
16	240	97.0	6387.0	0.8	1224.5	186299.0	1021.2 ± 6.0	86.67	2.72	0.082 ± 0.009
17	250	43.4	8464.0	0.0	1425.4	184939.1	902.5 ± 4.7	93.51	3.16	0.072 ± 0.008
18	270	84.3	7666.3	0.1	1603.8	211178.1	913.1 ± 4.8	89.45	3.56	0.090 ± 0.009
19	270	117.0	8362.6	0.0	1732.9	195479.9	807.3 ± 5.4	84.98	3.84	0.089 ± 0.011
20	270	70.7	9124.9	0.0	1850.2	197359.2	771.6 ± 3.5	90.43	4.10	0.087 ± 0.010
21	300	77.6	8566.2	0.0	1833.1	179769.8	720.3 ± 4.0	88.68	4.07	0.092 ± 0.011
22	300	80.6	7435.9	0.0	1421.5	125990.5	662.2 ± 4.2	84.10	3.15	0.082 ± 0.009
23	300	78.5	7473.2	0.0	1574.0	131895.8	631.7 ± 4.3	85.04	3.49	0.091 ± 0.010
24	350	59.7	7616.3	2.0	1481.8	119532.5	611.7 ± 4.2	87.14	3.29	0.084 ± 0.010
25	350	70.0	9321.2	0.7	1716.3	126015.5	564.5 ± 3.3	85.91	3.81	0.079 ± 0.008
26	370	67.7	8591.2	0.0	1501.6	104979.5	541.1 ± 4.1	83.99	3.33	0.075 ± 0.008
27	370	102.1	8104.4	0.0	1243.0	76593.9	484.8 ± 3.2	71.75	2.76	0.066 ± 0.009
28	350	102.7	7931.9	0.0	1280.1	78234.2	481.4 ± 5.0	72.05	2.84	0.069 ± 0.009
29	350	93.0	8005.7	0.2	1310.9	80992.1	486.0 ± 3.3	74.67	2.91	0.070 ± 0.008
30	350	82.2	8035.5	0.0	1208.7	73508.1	479.2 ± 3.1	75.16	2.68	0.065 ± 0.008
31	400	122.3	9325.9	1.4	1527.8	94252.2	485.3 ± 4.8	72.29	3.39	0.070 ± 0.007
32	400	56.8	8187.2	6.1	1369.3	83137.7	478.6 ± 2.9	83.20	3.04	0.072 ± 0.009
33	350	45.3	7533.9	2.2	1174.8	71902.8	481.9 ± 3.2	84.30	2.61	0.067 ± 0.008
34	350	56.4	8076.7	2.5	1250.4	74877.2	472.8 ± 3.4	81.79	2.77	0.067 ± 0.007
35	350	44.1	8004.8	8.4	1193.7	71471.8	472.7 ± 6.6	84.59	2.65	0.064 ± 0.007
36	400	50.9	9822.7	3.2	1423.3	84833.1	470.9 ± 3.9	84.93	3.16	0.062 ± 0.007
37	350	30.8	8533.6	3.7	1243.9	73564.5	467.6 ± 5.6	88.99	2.76	0.063 ± 0.007
38	350	29.6	8201.2	0.4	1292.6	77531.0	473.5 ± 4.0	89.87	2.87	0.068 ± 0.007
39	350	56.4	8367.8	3.4	1244.1	73223.6	465.7 ± 3.6	81.47	2.76	0.064 ± 0.008
40	400	56.9	9571.3	1.6	1406.4	83021.1	466.9 ± 3.5	83.15	3.12	0.063 ± 0.007
41	450	40.9	9563.7	5.7	1434.8	85247.4	469.5 ± 2.5	87.59	3.18	0.065 ± 0.007
42	500	83.7	10613.9	3.1	1511.1	89879.2	470.0 ± 5.2	78.43	3.35	0.061 ± 0.007

These $^{40}Ar/^{39}Ar$ experiments were measured using a quadrupole mass spectrometer at VU University Amsterdam. The argon isotopes are listed in counts per second (cps).

Table 5.2 Complete ^{40}Ar/^{39}Ar crushed powder stepped heating data

Step	T(°C)	$^{36}Ar_{air}$	$^{37}Ar_{Ca}$	$^{38}Ar_{Cl}$	$^{39}Ar_{K}$	^{40}Ar*	Age ± 2σ (Ma)	$^{40}Ar_{K}$ (%)	$^{39}Ar_{K}$ (%)	K/Ca(±2σ)
(a).Amphibole 09NQ13Amp, by stepwise heating, J = 0.005037										
1	300	1032.2	29433.9	15.8	12668.6	593595.2	382.3 ± 2.0	28.33	2.66	0.185 ± 0.019
2	350	2015.9	14147.5	42.9	5727.6	235519.8	339.6 ± 7.8	66.06	5.88	0.174 ± 0.019
3	400	1699.2	17630.2	70.6	5980.0	242015.2	334.7 ± 6.0	32.52	2.78	0.146 ± 0.016
4	450	1579.1	21254.1	51.8	6754.3	259115.1	318.7 ± 4.8	35.70	3.14	0.137 ± 0.017
5	550	1521.0	31424.0	71.3	9247.7	407232.5	361.4 ± 6.8	47.54	4.29	0.127 ± 0.013
6	600	2065.1	35735.6	80.8	9835.0	451296.9	375.1 ± 4.1	42.51	4.57	0.118 ± 0.013
7	650	3074.3	52962.9	126.9	12147.8	607088.9	405.1 ± 4.3	40.66	6.15	0.099 ± 0.010
8	750	3846.4	100014.9	247.5	19092.3	986969.4	417.5 ± 3.4	44.58	9.39	0.082 ± 0.008
9	850	5769.6	373530.1	452.3	58739.1	2577524.3	360.3 ± 2.2	62.50	27.85	0.068 ± 0.007
10	900	9774.9	423760.1	596.8	71283.0	2156061.1	255.8 ± 2.6	42.45	33.31	0.072 ± 0.007
(b).Amphibole 09NQ29Amp, by stepwise heating, J = 0.005031										
1	300	674.7	30623.5	6.4	8887.9	369100.3	340.6 ± 2.2	64.93	8.35	0.125 ± 0.013
2	400	1581.6	17060.5	26.5	4275.9	141523.9	276.4 ± 8.0	23.24	4.02	0.108 ± 0.012
3	450	1515.2	22699.5	36.6	4481.1	143131.7	267.5 ± 7.0	24.22	4.21	0.085 ± 0.010
4	500	1508.8	24914.2	69.0	5070.9	149727.0	248.6 ± 5.6	25.14	4.77	0.088 ± 0.011
5	550	2467.5	29992.9	102.8	5495.2	163851.1	250.8 ± 7.8	18.35	5.16	0.079 ± 0.008
6	600	2731.5	33184.9	79.3	5862.2	181332.0	259.6 ± 8.5	18.34	5.51	0.076 ± 0.008
7	650	2801.7	66477.0	88.7	7292.3	297638.5	335.2 ± 6.8	26.44	6.85	0.047 ± 0.005
8	700	2767.6	81856.7	83.1	7038.9	283340.1	331.0 ± 7.9	25.73	6.62	0.037 ± 0.004
9	750	3233.9	133252.4	137.6	8721.9	427645.7	395.8 ± 6.1	30.92	8.20	0.028 ± 0.003
10	800	4010.9	335260.5	189.2	17076.4	877643.6	412.8 ± 4.3	42.54	16.05	0.022 ± 0.002
11	850	8663.3	297400.7	293.7	14142.9	448258.2	265.5 ± 10.6	14.90	13.29	0.020 ± 0.002
12	900	11315.3	412001.2	397.7	18056.8	426914.1	201.7 ± 11.2	11.32	16.97	0.019 ± 0.002

These ^{40}Ar/^{39}Ar experiments were measured using a quadrupole mass spectrometer at VU University Amsterdam. The argon isotopes are listed in cps.

The ^{40}Ar/^{39}Ar dating results of amphibole separates 09NQ13Amp and 09NQ29Amp by *in vacuo* crushing yields similar monotonically decreasing staircase-shaped age spectra characterized by anomalously high apparent ages in the initial steps (Figure 5.2a and c). Subsequently, upon continued crushing, the apparent ages gradually stabilize to reveal age plateaus. After applying the initial ^{40}Ar/^{36}Ar ratios from atmospheric air as 295.5 to exclude the non-radiogenic ^{40}Ar, the two amphibole samples produce relatively concordant apparent ages in the final steps with Early Palaeozoic weighted mean ages of 487.9 ± 6.5 Ma (^{39}Ar=47.6%，MSWD=190) and 475.7 ± 3.6 Ma (^{39}Ar=46.8%，MSWD=14.8), respectively (Figure 5.2a and c). The data points of the steps defining the above ages yield isochrons with younger ages of 469 ± 2.1 Ma and 462.6 ± 3.6 Ma, corresponding to initial ^{40}Ar/^{36}Ar ratios of 519.9 ± 20.1 and 333.8 ± 9.5 (Figure 5.2b and d). These results indicate that there is a significant amount of excess ^{40}Ar present within the small primary fluid inclusions that survive in the powdered mineral separates after crushing.

All crushed residual powders were subsequently investigated by means of stepwise heating. In comparison to the *in vacuo* crushing experiments, the ^{40}Ar/^{39}Ar dating results by stepwise heating yield relatively complicated age spectra and younger apparent ages. Saddle shaped age spectra with minimum apparent ages of 319 and 249 Ma at temperatures of 450 °C and 500 °C, and maximum apparent ages of 418 and 413 Ma at temperatures of 750 °C and 800 °C are obtained from samples 09NQ13Amp and 09NQ29Amp, respectively

(Figure 5.2a and c). There is too much scatter in the data of all amphibole samples to form well-defined isochrons (Figure 5.2b and d).

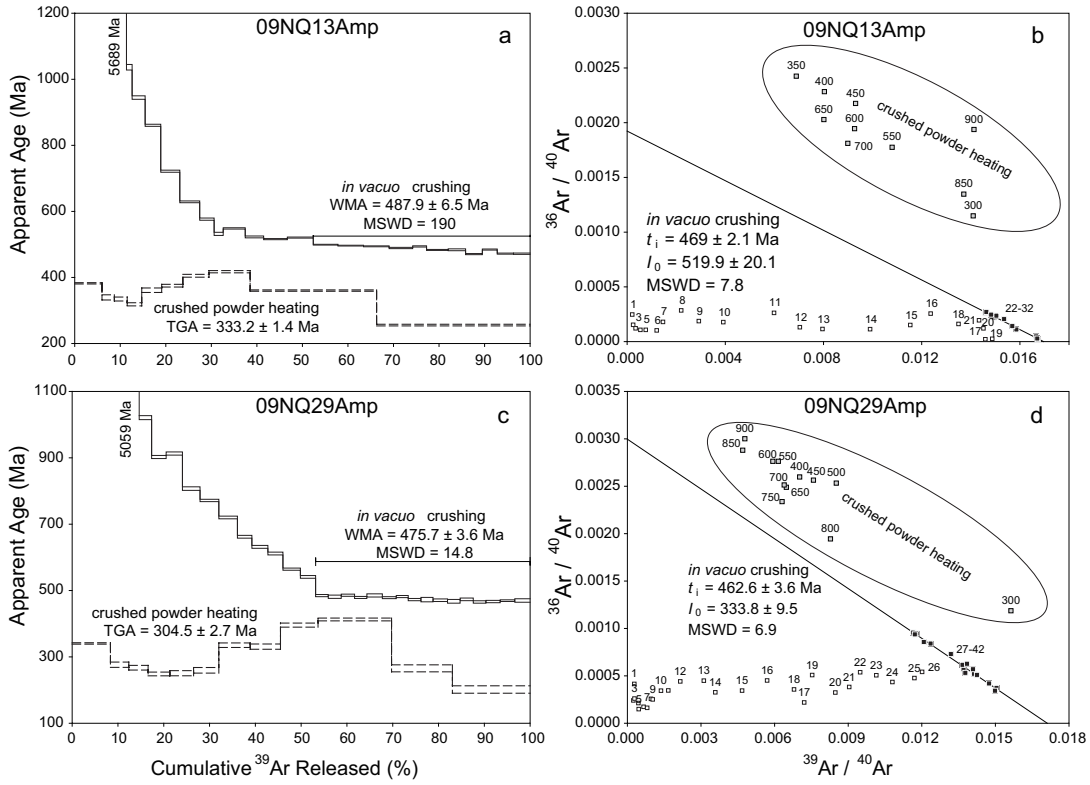

Figure 5.2 Plots of the age spectra (a, c) and inverse isochrons (b, d) of amphibole based on the $^{40}Ar/^{39}Ar$ results by *in vacuo* crushing and crushed powder stepwise heating. The distributions of the data points in the inverse isochrons have features in common. The results of crushing gradually move away from the excess ^{40}Ar end-member to the radiogenic ^{40}Ar end-member, indicating that the excess argon (Ar_E) and radiogenic argon (Ar_R) contribute successively to different parts of the degassing. In contrast, the data points from stepwise heating experiments show a radiogenic ^{40}Ar end-member to air ^{40}Ar end-member trend with increasing heating temperature, but they are too scattered to form well-correlated linear arrays. The crushing data points contributing to the weighted mean ages define isochron lines with intercept ages of 469 and 463 Ma. Here, WMA stands for weighted mean age and TGA is the total gas age.

5.4 Discussion

5.4.1 The source of Ar isotopes in the fluid inclusions

To search for elemental correlations, we performed multiple regressions on the amount of $^{40}Ar^*$, Cl ($^{38}Ar_{Cl}$) and K ($^{39}Ar_K$) with the aim of identifying the different Ar sources in the fluid inclusions (Kelley et al., 1986; Kendrick et al., 2001; Qiu and Wijbrans, 2006). Here, $^{40}Ar^*$ denotes total ^{40}Ar minus atmospheric ^{40}Ar ($^{40}Ar_A$). In other words, $^{40}Ar^*$ includes both *in situ* derived radiogenic ^{40}Ar ($^{40}Ar_R$) from the decay of ^{40}K and parentless excess ^{40}Ar ($^{40}Ar_E$).

The plots of $^{39}Ar_K/^{38}Ar_{Cl}$ vs. $^{40}Ar^*/^{38}Ar_{Cl}$ based on isotopic analysis of two amphibole samples by crushing are shown in Figure 5.3. Due to the presence of multiple generations of

fluid inclusions, representing different stages of fluid infiltration, the data points of the first several steps show high $^{40}Ar^{*}/^{38}Ar_{Cl}$ ratios and the complete data set is too scattered to form correlation lines. In contrast, the data points that contribute to the age plateaux, indicated in dark in Figure 5.3, define correlation lines with slopes corresponding to ages of 495 Ma (09NQ13Amp) and 485 Ma (09NQ29Amp), respectively. The correlation lines with $^{38}Ar_{Cl}$ suggest that the components released by crushing are extracted from halogen-bearing hydrous fluid inclusions. If the liberated gases were mixtures of more than two end members with different origins, distinct initial $^{40}Ar/^{36}Ar$ ratios and different proportional argon release patterns, such as gas from mineral inclusions or the crusher, a flat age plateau and an isochron could never be obtained (Qiu and Wijbrans, 2009). In other words, the air-component end member shown in the isochron plots of $^{39}Ar_K/^{38}Ar_{Cl}$ vs. $^{40}Ar^{*}/^{38}Ar_{Cl}$ (Figure 5.3) is derived from hydrous fluid inclusions in amphibole rather than an artifact caused by release of argon from the metal of the crusher.

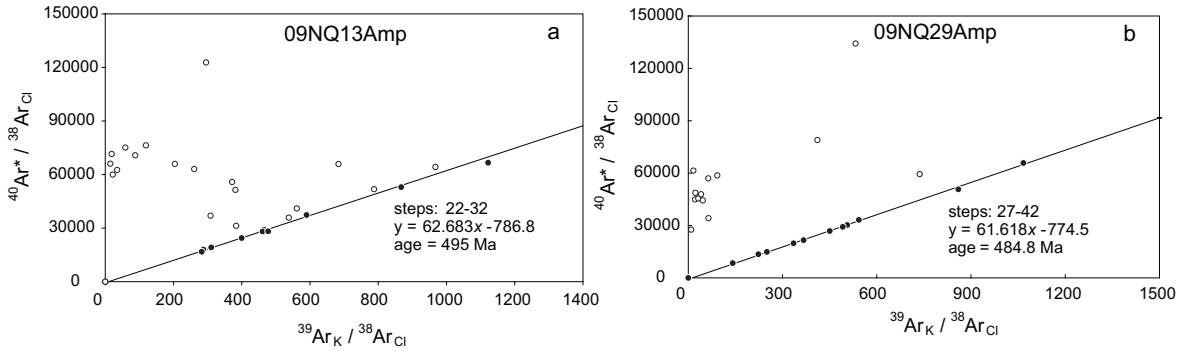

Figure 5.3 Plots of $^{39}Ar_K$ /38Ar_{Cl} vs. $^{40}Ar^{*}/^{38}Ar_{Cl}$ based on the *in vacuo* crushing $^{40}Ar/^{39}Ar$ data of amphibole samples. The solid symbols are those defining the age plateaux, and in this diagram define correlation lines with slopes corresponding to ages of 495 (09NQ13Amp) and 485 Ma (09NQ29Amp).

The plots of $^{40}Ar^{*}/^{39}Ar_K$ vs. $^{38}Ar_{Cl}/^{39}Ar_K$ based on the $^{40}Ar/^{39}Ar$ data of the amphiboles by crushing are shown in Figure 5.4 and reveal the following characteristics:

(1) The initial crushing steps (open symbols with labels in Figure 5.4) yield clear linear correlations with $^{40}Ar^{*}/^{39}Ar_K$ intercepts of 41-35.2, corresponding to ages of 337-295 Ma (Figure 5.4). The intercept ages (337-295 Ma) can probably be taken as the best estimate for the age of secondary fluid inclusions (SFIs), as discussed later.

(2) In contrast, the late crushing steps (dark symbols near the origin of Figure 5.4) define the isochrons without any correlation between $^{40}Ar^{*}/^{39}Ar_K$ and $^{38}Ar_{Cl}/^{39}Ar_K$, but with constant low $^{40}Ar^{*}/^{39}Ar_K$ ratios, implying a unique reservoir dominates the degassing. Two amphibole samples show average $^{40}Ar^{*}/^{39}Ar_K$ ratios of 63-59 and average ages of 485 and 475 Ma, respectively (Figure 5.4a, b). These ages are based on the data from the late crushing steps and are interpreted as the contributions of the primary fluid inclusions (PFIs).

(3) In addition to that, we note that the crushing steps (gray symbols in Figure 5.4) between the initial and final crushing steps have low $^{40}Ar^{*}/^{39}Ar_K$ ratios, low $^{38}Ar_{Cl}/^{39}Ar_K$ ratios,

and a scattered distribution. These ratios are interpreted to indicate that the gases in these crushing steps were a mixture with variable proportions of the PFI and SFI end members.

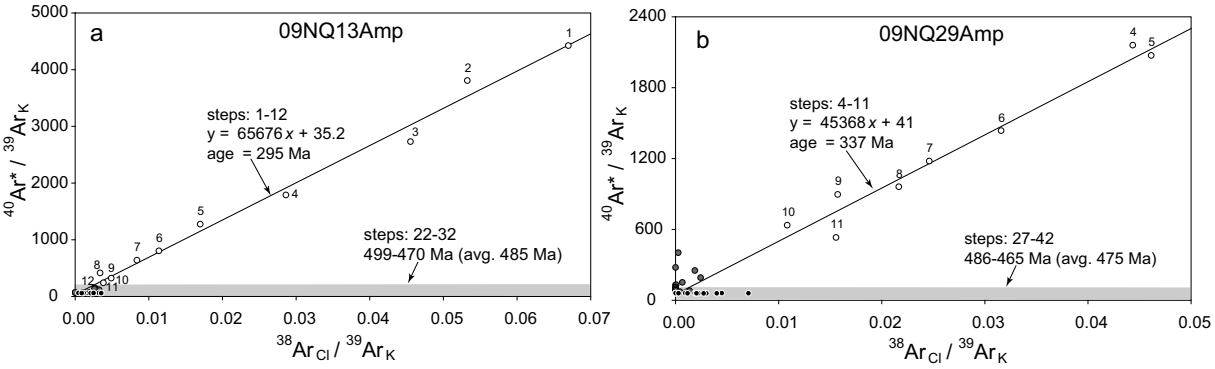

Figure 5.4 Plots of the correlation between $^{40}Ar^{*}/^{39}Ar_K$ vs. $^{38}Ar_{Cl}/^{39}Ar_K$ for *in vacuo* crushing of amphiboles (a, b). $^{40}Ar^{*}$ shows strong correlation with $^{38}Ar_{Cl}$ in the early crushing steps of all the samples. Data points of open symbols are used to the inverse isochron age calculation while the gray symbols are excluded from the isochrons. Data points that defining the age plateaux shown by dark symbols.

5.4.2 Dating episodic flow of metamorphic fluid

Fluid flow in UHP metamorphic terranes is generally considered to be episodic (Zheng, 2004). The *PT*-evolution of eclogites in the Yuka terrane can be divided into four metamorphic stages: pre-eclogite-facies, peak pressure, initial retrograde stage and post peak-*T* retrogression (Figure 5.5, chapters 3 and 4). Therefore, Yuka HP/UHP minerals corresponding to the various metamorphic stages could have encapsulated fluid inclusions with a variety of ages and origins during the mineral growth.

The purpose of the *in vacuo* crushing technique is to extract the Ar-bearing gas that was trapped in fluid inclusions and in inclusions along sealed cracks and cavities in crystals. Previous studies have shown that crushing has little effect on the gas trapped within the crystal lattice (Dunlap and Kronenberg, 2001; Qiu et al., 2002; Qiu and Wijbrans, 2006; 2008; Jiang et al., 2012; Bai et al., 2013). An exception to this may be scapolite (Kendrick and Phillips, 2009), for which argon release by crushing was described. This may be due to the relatively open crystal structure of scapolite where volatiles may have been trapped in cavities within the crystal lattice. In most cases, the results of the $^{40}Ar/^{39}Ar$ *in vacuo* crushing should reflect the age information of the fluid flow as recorded by fluid inclusions in amphiboles and quartz that crystallized during amphibolite-facies to greenschist-facies retrogression.

5.4.3 Implications of gas release patterns and spectra of crushing experiments

5.4.3.1 Gas release pattern

The new results from amphibole $^{40}Ar/^{39}Ar$ *in vacuo* crushing analysis all yield descending staircase-shaped age spectra with anomalously high initial apparent ages in the first few

steps and relatively flat age plateaux over the final several steps. Following the interpretation of Qiu and Wijbrans (2006; 2008) we suggest that the extremely high initial apparent ages are derived from the largest, most easily crushed secondary fluid inclusions (SFIs) that are dominated by excess ^{40}Ar and that were most likely incorporated in the amphibole and quartz after the initial amphibolite-facies conditions. Meanwhile, in the diagrams of Figure 5.4, we discovered that the $^{40}Ar^{*}$(representing $^{40}Ar_R$+$^{40}Ar_E$) shows a good correlation with $^{38}Ar_{Cl}$ in the initial crushing steps, implying the excess ^{40}Ar in the SFIs and Cl came from the same source. With continued crushing, the apparent ages decrease gradually probably reflecting a mixture between SFIs with excess ^{40}Ar and PFIs. Finally, once the high-excess ^{40}Ar reservoir is exhausted, subsequent gas components are mainly derived from smaller PFIs. During this stage of the experiment a relative flat age plateau is formed over the final several steps. The amphibole data points constituting the age plateaus result in isochrons with relatively young intercept ages (469-463 Ma), corresponding to initial ^{40}Ar/^{36}Ar values from 334 to 520, implying excess ^{40}Ar is also present in the fine PFIs of amphibole samples.

In an alternative model to explain the results of Qiu and Wijbrans (2006; 2008) on the release patterns of Bixiling by stepwise crushing, Kendrick (2007) postulated the presence of small sericite crystals (~10 μm) dispersed throughout the host garnet that contributed to the release of radiogenic argon after prolonged crushing as the source of the observed age plateaus. Although this is a plausible model, it critically hinges upon the presence of fine sericite evenly dispersed throughout the crystals used for crushing. In the case of the Bixiling garnets, Qiu and Wijbrans pointed out that in these garnets they have found no evidence for such sericite inclusions whereas the presence of numerous small primary fluid inclusions was demonstrated. Moreover, for the case of Bixiling garnet inclusions Qiu and Wijbrans pointed out that the radiogenic component had a positive correlation with the $^{38}Ar_{Cl}$ concentration, which would point to a chloride enriched reservoir that was releasing the radiogenic argon signal. A chloride-enriched radiogenic argon signal is considered to be more consistent with an inclusion-hosted brine source than with a mica crystal source. For the present study sericite inclusions in amphibole are considered an unlikely source for the radiogenic signal as sericite is not normally part of mafic amphibolite mineral assemblages.

Amphibole is mainly formed during amphibolite facies and greenschist facies retrogression. During these stages, significant amounts of fluid could be obtained from molecular H_2O in nominally anhydrous minerals like garnet and omphacite, the breakdown of hydrous minerals like zoisite, phengite and lawsonite, the exsolution of hydroxyl minerals (Zheng et al., 2003; Zheng, 2004; Song et al., 2005a; Frezzotti et al., 2007; Wu et al., 2009b), and even from the host gneiss (Chen et al., 2007b; Zong et al., 2010). As a consequence, this kind of metamorphic fluid probably was trapped by amphibole and vein quartz crystals during crystallization or at a later stage by a crack-seal mechanism. Such fluid inclusions can therefore be considered primary. The ages of these PFIs therefore not only record aqueous

fluid flow during the exhumation stages of HP/UHP rocks, but can also be taken as the best estimate for the ages of amphibolite facies retrogression and quartz-vein formation.

5.4.3.2 Implications of crushing spectra

Crushing experiments of two amphibole samples yielded $^{40}Ar/^{39}Ar$ isochron ages of 469 ± 2.1 and 462.6 ± 3.6 Ma. These ages are consistent with the $^{40}Ar/^{39}Ar$ stepwise heating isochron ages (477-466 Ma) from eclogite phengite and amphibole that have been interpreted as the timing of early cooling in the eclogite facies after peak pressure metamorphism (Zhang et al., 2005a)(also see chapter 4). This suggests that the $^{40}Ar/^{39}Ar$ ages of 469-463 Ma constrain the age of fluid flow responsible for initial amphibolite-facies retrogression during the exhumation of the UHP rocks (Figure 5.5). On the other hand, the granite zircon U-Pb dating from the Da Qaidam region performed by various analytical techniques produced ages from 397 Ma to as old as 490 Ma with a cluster in the range 465-463 Ma, which have been interpreted to date intrusion of regionally widespread Ordovician plutons (Gehrels et al., 2003; Wu et al., 2007). Therefore, regional syn-exhumation arc-magmatism accompanied by the release of aqueous fluid may be an alternative explanation for enhanced fluid flow at 469-463 Ma.

5.4.3.3 Implications of gas release patterns and spectra of stepwise heating

The two amphibole samples have similar saddle-shaped age spectra, which have commonly been attributed to the presence of excess argon and partial resetting or contamination by other phases (Harrison and McDougall, 1981; Harrison and Fitzgerald, 1986). The relatively young apparent ages (418-249 Ma) and total gas ages (333-305 Ma) obtained from two amphibole samples are much younger than the published amphibole $^{40}Ar/^{39}Ar$ incremental heating result of 477 Ma (Zhang et al., 2005a). This indicates that the saddle shaped release patterns are not caused by variable incorporation of excess ^{40}Ar. Otherwise, the apparent ages at the initial and/or last steps should be older than the age of 477 Ma. The obvious presence of mineral inclusions such as biotite, feldspar, and quartz in amphibole porphyroblasts, characterized by various shapes and sizes from 0.01 mm to 0.1 mm, suggests that mineral inclusions may have played a role in producing the complicated release patterns during stepwise heating of the residual powder after crushing. The 319-249 Ma apparent ages obtained at heating temperatures around 500 °C probably represent the formation or resetting ages of late retrograde minerals, whereas the apparent ages of 418-413 Ma, obtained at heating temperatures around 800 °C, may represent amphibolite cooling ages. On balance, based upon the young apparent ages from the stepwise heating experiments, we suggest that there is no excess ^{40}Ar in the amphibole crystals or their mineral inclusions, and that almost all excess ^{40}Ar is hosted in primary and secondary fluid inclusions.

Considering all *in vacuo* crushing and residual powders stepwise heating results, we suggest that amphibole in the Yuka amphibolites crystallized at *ca.* 469-463 Ma, and then cooled below the amphibole K-Ar system closure temperature of about 500 ± 50 °C (Harrison,

1982) at or before 418 Ma (09NQ13Amp) and 413 Ma (09NQ29Amp), i.e. the maximum ages in in the plateau (see Figure 5.2a and c).

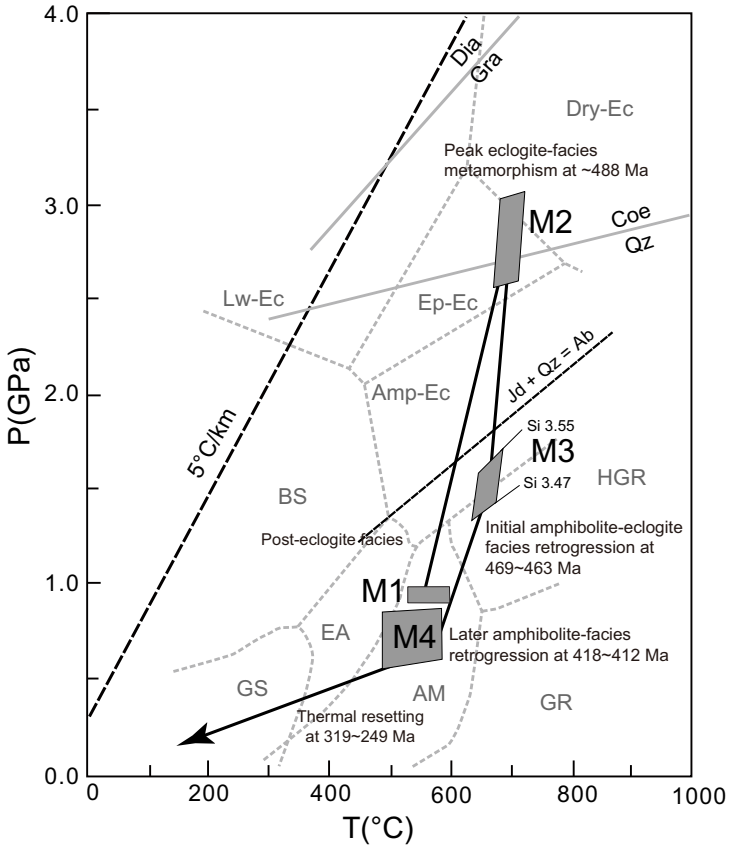

Figure 5.5 *Pressure-temperature-time (P-T-t)* path for eclogite from the Yuka terrane, North Qaidam UHP metamorphic belt, Western China, amended with our new ages for fluid flow events (modified from chapter 3 and 4). M1: an earlier pre-eclogite-facies stage; M2: peak pressure stage; M3: an initial retrograde stage; M4: a later stage of retrogression stage. Facies boundaries are from Liou et al. (1998).

5.5 Conclusions

An investigation of ^{40}Ar/^{39}Ar dating by *in vacuo* crushing and stepwise heating of amphibole separates from amphibolite-facies overprinted HP/UHP metamorphic rocks from the Yuka terrane resulted in the following conclusions:

1. The ^{40}Ar/^{39}Ar *in vacuo* crushing technique appears to be an effective and promising approach to directly date the mineral formation ages in retrogressed HP/UHP rocks and to decipher the occurrence of excess ^{40}Ar. In addition, gas trapped in solid inclusions in minerals could be liberated by subsequent stepped heating analysis of the crushed powder and provide useful geological information about the retrograde metamorphic overprinting of HP/UHP rocks.

2. *In vacuo* crushing $^{40}Ar/^{39}Ar$ analysis was applied to amphibole separates from two amphibolite samples from the Yuka HP/UHP terrane in Western China. The results indicate that the secondary fluid inclusions were formed subsequent to UHP metamorphism and that the amphibole and quartz incorporated significant amounts of heterogeneous excess ^{40}Ar in fluid inclusions. The excess ^{40}Ar is generally released early in the crushing experiments. Primary fluid inclusions trapped during amphibole growth and released during the later stages of the crushing experiments contain relatively homogeneous excess ^{40}Ar.
3. *In vacuo* crushing of amphibole provides a geochronological record of episodes of fluid flow with ages ranging from 469 to 463 Ma, reflecting the timing of the Yuka eclogite initial amphibolite-facies retrogression.
4. Based on the $^{40}Ar/^{39}Ar$ stepwise heating ages of amphibole residual powders and their equilibration and closure temperatures, we deduce that the Yuka metamorphic complex and its country rocks cooled from peak metamorphic temperature to 500 ± 50 °C and reached medium to upper crustal levels at or before 418-413 Ma. The K-Ar isotope system in amphibole was partially reset by later tectonothermal events at *ca.* 319 to 249 Ma, indicating that the Yuka eclogites and the products of their retrogression were overprinted by multiple later thermal events in the Silurian and possibly as young as the Triassic.